REGION-OF-INTEREST RECONSTRUCTION FROM PROJECTIONS USING EXPONENTIAL RADIAL SAMPLING

Berkman Sahiner and Andrew E. Yagle

Dept. of EECS, The University of Michigan, Ann Arbor, MI 48109-2122 aey@eecs.umich.edu

ABSTRACT

We combine several ideas, including nonuniform sampling and circular harmonic expansions, into a new procedure for reconstructing a small region of interest (ROI) of an image from a set of its projections that are densely sampled in the ROI and coarsely sampled outside the ROI. Specifically, the radial sampling density of both the projections and the reconstructed image decreases exponentially with increasing distance from the ROI. The problem and data are reminiscent of the recently-formulated local tomography problem; however, our algorithm reconstructs the ROI of the image itself, not the filtered version of it obtained using local tomography. The new algorithm has the added advantages of speed (it can be implemented entirely using the FFT) and parallelizability (each image harmonic is independent).

1. INTRODUCTION

The problem of image reconstruction from a complete set of projections is to compute an image $\mu(x,y)$ from its Radon transform, i.e., from a complete set of its line integrals $p(r,\theta)$, defined as

$$p(r,\theta)=\int_{-\infty}^{\infty}\int_{-\infty}^{\infty}\mu(x,y)\delta(r-x cos\theta-y\sin\theta)dxdy. \quad (1)$$

The most common procedure for reconstruction from a complete set of projections is filtered backprojection (FBP). In FBP the projections $p(r,\theta)$ are first filtered with a filter $h(r)$ whose Fourier transform $\hat{h}(w)\approx|w|$ up to some cutoff frequency, and is windowed to zero for higher frequencies. These filtered projections are then backprojected. When the projections are sampled in the angular and radial variables, but cover the entire extent of the image, FBP still yields quite satisfactory results. The resolution of the reconstructed image is determined by the sampling densities in r and θ of $p(r,\theta)$ and the cutoff frequency of $\hat{h}(w)$.

In many applications, it is not possible to obtain a complete set of projections which are sampled densely enough to attain the desired resolution over the entire support of $\mu(x,y)$ [1]. For example, X-ray dose limitations, or time constraints when imaging a moving object, may preclude such a large number of projections. If the entire support of $\mu(x,y)$ is covered, but projections are not sampled densely enough, then the desired resolution is not attained. If the projections are dense enough around some region of interest (ROI) of $\mu(x,y)$, but do not cover the entire support of $\mu(x,y)$, then a good reconstruction using FBP is not possible, due to the infinite support of the filter $h(r)$ [1] (ideally $h(r)$ is a derivative-Hilbert transform $\mathcal{H}d/dr$).

An example of image reconstruction from incomplete data is local tomography [2], in which the filter $h(r)$ no longer approximates $\mathcal{H}d/dr$. The local filter $h(r)=d^2/dr^2+\alpha\delta(r)$ is used, and the Fourier transform $\hat{\tilde{\mu}}(w_1,w_2)$ of the reconstructed image $\tilde{\mu}(x,y)$ is related to the Fourier transform $\hat{\mu}(w_1,w_2)$ of $\mu(x,y)$ by $\hat{\tilde{\mu}}(w_1,w_2)=\sqrt{w_1^2+w_2^2}\hat{\mu}(w_1,w_2)+\alpha\hat{\mu}(w_1,w_2)/\sqrt{w_1^2+w_2^2}$. The idea is that since this $h(r)$ is local, only projections passing through the ROI are used; no other projections need be taken. However, it is clear that $\tilde{\mu}(x,y)\neq\mu(x,y)$; for example, constant regions of $\mu(x,y)$ tend to become cup-shaped functions $\tilde{\mu}(x,y)$ [2]. Furthermore, local tomography is even more susceptible to noise than FBP, due to the extra noise-amplifying $\sqrt{w_1^2+w_2^2}$.

In this paper, we introduce a different type of region-of-interest tomography, based on exponential radial sampling of the image and projections. We assume that we are interested in obtaining high resolution only in a small ROI; outside this region, high resolution is not very important. Without loss of generality, we assume that the ROI is centered on the origin (this can easily be achieved by translating $\mu(x,y)$). The angular sampling is conventional equiangular sampling, i.e., $p(r,\theta)$ is sampled in θ at angles $\theta_n=\frac{2\pi}{N}n$, $n=0,1,\ldots,N-1$. However, the radial sampling in r in $p(r,\theta)$ and ρ in $\mu(x,y)=\mu(\rho,\phi)$ (polar coordinates) is exponential, i.e., $p(r,\theta)$ is sampled in r at distances $r_k=r_1e^{(k-1)\Delta}, k\geq 1$.

This means that the samples are very dense around the origin (i.e., in the ROI), and the sampling density decreases exponentially with increasing distance from the origin. This gives us good resolution around the origin (in the ROI), and poor resolution far away from the origin (which is irrelevant). These remarks apply both to the data (the projections $p(r,\theta)$) and the reconstructed image $\mu(\rho,\phi)$. Although the exponential decrease of sampling density with increasing r is not as sharp as the abrupt drop of sampling density to zero in local tomography or the interior problem, it is quite steep, regardless of the value of Δ, and it is clearly in the spirit of localizing the projection data in a ROI. It shares the advantages of local tomography (viz., using less data, with attendant smaller X-ray exposure). And it has a significant advantage over local tomography: $\mu(x,y)$, not $\tilde{\mu}(x,y)$, is computed in the ROI.

Exponential nonuniform sampling calls to mind the wavelet transform, which has been used recently [3] to obtain a different type of reconstruction algorithm using nonuniform

This work was supported by the Office of Naval Research under Young Investigator grant #N00014-90-J-1897.

sampling. It is interesting to compare our numerical results to those of [3], although the approaches and data required are quite different. For example, our approach is exact to discretization, the error due to which can be made arbitrarily small, while the approach of [3] requires wavelet basis functions with compact support both before and after a derivative-Hilbert transform, which clearly cannot be found (although functions with rapidly decaying support can be found). Our approach is related to the wavelet transform, but in a completely different way from [3]–it generalizes to a convolution in scale (see [4]).

For image reconstruction using exponential radial sampling, we use the circular harmonic decomposition, which is a Fourier expansion in the angular variable θ or ϕ. This decomposition has been applied to reconstruction from projections in [5]. However, [5] used either continuous variables or uniform sampling, while we use exponential radial sampling. This creates two advantages: (1) it results in a region-of-interest tomography problem, as described above; and (2) the reconstruction formula can be written as a regular convolution for each harmonic. Since the fast Fourier transform (FFT) can be used to implement these convolutions, all in parallel, this results in a reconstruction algorithm that is an order of magnitude faster than FBP.

2. CIRCULAR HARMONIC IMAGE RECONSTRUCTION

Let $\mu(\rho,\phi)$ denote the image in polar coordinates. Since both the image and its projection $p(r,\theta)$ are periodic in the angular variable with period 2π, they can be expanded in Fourier series (circular harmonic decompositions [5])

$$\mu(\rho,\phi)=\sum_{n=-\infty}^{\infty}\mu_n(\rho)e^{jn\phi};\quad p(r,\theta)=\sum_{n=-\infty}^{\infty}p_n(r)e^{jn\theta}, \tag{2}$$

where

$$\mu_n(\rho)=\frac{1}{2\pi}\int_0^{2\pi}\mu(\rho,\phi)e^{-jn\phi}d\phi;\, p_n(r)=\frac{1}{2\pi}\int_0^{2\pi}p(r,\theta)e^{-jn\theta}d\theta \tag{3}$$

are the circular harmonics of $\mu(\rho,\phi)$ and $p(r,\theta)$.

Circular harmonics of the image can be reconstructed from circular harmonics of the projections, independently for each n [5]. In this paper we use the "noncausal, stable" form of circular harmonic reconstruction [5]:

$$\mu_n(\rho)=\frac{1}{\pi}\left[\int_0^{\rho}U_{n-1}(\frac{r}{\rho})-\int_{\rho}^{\infty}\frac{e^{(-n\cosh^{-1}(r/\rho))}}{\sqrt{r^2-\rho^2}}\right]p_n'(r)dr, \tag{4}$$

where $U_n(x)=\sin((n+1)\cos^{-1}x)/\sin(\cos^{-1}x)$ is the Chebyshev polynomial of the second kind of order n. Note that (4) is DIFFERENT from the original "causal, unstable" Cormack formula, whose integrand was unbounded for large n. In (4) the integrand is bounded as $n\to\infty$. (4) has been used [5] to perform fairly accurate reconstructions from regularly sampled projections.

3. DERIVATION OF THE ALGORITHM

3.1. Problem Specification

The problem that we solve in this section is defined as follows. Given samples of the projections of an image, where the sampling density is exponential in the radial variable and equiangular in the angular variable, compute the image on the same grid. That is, given $\{p(r_k,\theta_n), r_k = r_1e^{(k-1)\Delta}, k=1,\ldots,K;\theta_n=\frac{2\pi}{N}n, n=0,1,\ldots,N-1\}$, compute $\{\mu(\rho_k,\phi_n)\}$ for analogous values of ρ_k and ϕ_n. For convenience we define $r_0=\rho_0=0$.

We assume that: (1) the image (and hence the projections also) is known to have its support inside a disk of radius R; and (2) the image (and hence the projections also) is known to have only N circular harmonics $\mu_n(\rho)$ significantly different from zero. $r_1=\rho_1$ is the smallest radius of interest, and $r_K=\rho_K=R$, so that $(K-1)\Delta=\ln(R/r_1)$. Note that the grid is very dense around r_1, and much sparser around r_K, dropping off exponentially with increasing radius, regardless of the size of Δ.

3.2. Discretization

We first discuss how to obtain the harmonics $\mu_n(\rho)$ of the image from the harmonics $p_n(r)$ of the projections. Since $\mu_{-n}(\rho)=\mu_n^*(\rho)$, we require image harmonics only for $n\geq 0$. Changing variables from r to $x=\cos^{-1}(r/\rho)$ in the first integral of (4) and $x=\cosh^{-1}(r/\rho)$ in the second integral of (4), and substituting $\rho=\rho_j$, (4) can be written as [5]

$$\begin{aligned}\mu_n(\rho_j) &= \frac{1}{\pi}\int_0^{\pi/2}\sin(nx)p_n'(\rho_j\cos x)dx\\ &- \frac{1}{\pi}\int_0^{\cosh^{-1}(R/\rho_j)}e^{-nx}p_n'(\rho_j\cosh x)dx\\ &= \frac{1}{\pi n}\int_{x=0}^{x=\pi/2}p_n'(\rho_j\cos x)d(\cos nx)\\ &+ \frac{1}{\pi n}\int_{x=0}^{x=\cosh^{-1}(R/\rho_j)}p_n'(\rho_j\cosh x)d(e^{-nx})\end{aligned} \tag{5}$$

We now generalize the result of [5]. Instead of choosing fixed discretization points $\{x_{j,k}\}$ to approximate (5) as in [5], we let $\{x_{j,k}\}_{k=0}^{K}$ be any real numbers such that

$$\begin{aligned}0=x_{j,j}\leq x_{j,j-1}\leq\ldots\leq x_{j,0}=\pi/2\\ 0=x_{j,j}\leq x_{j,j+1}\leq\ldots\leq x_{j,K}=\cosh^{-1}(R/\rho_j).\end{aligned} \tag{6}$$

Then, following an argument analogous to the argument in [5], it is easily shown that a first approximation to (5) is

$$\begin{aligned}\mu_n(\rho_j) &= \frac{1}{\pi n}\sum_{k=0}^{j-1}a_{n,j}(k)\left(\cos(nx_{j,k+1})-\cos(nx_{j,k})\right)\\ &+ \frac{1}{\pi n}\sum_{k=j}^{K-1}a_{n,j}(k)\left(e^{-nx_{j,k+1}}-e^{-nx_{j,k}}\right)\end{aligned} \tag{7}$$

where $a_{n,j}(k)$, which approximates $p_n'(\rho_j\cos x)$ or $p_n'(\rho_j\cosh x)$, is defined as

$$a_{n,j}(k) = \begin{cases} \dfrac{p_n(\rho_j \cos x_{j,k+1}) - p_n(\rho_j \cos x_{j,k})}{\rho_j \cos x_{j,k+1} - \rho_j \cos x_{j,k}}, & 0 \le k < j \\ \dfrac{p_n(\rho_j \cosh x_{j,k+1}) - p_n(\rho_j \cosh x_{j,k})}{\rho_j \cosh x_{j,k+1} - \rho_j \cosh x_{j,k}}, & j \le k < K. \end{cases} \quad (8)$$

3.3. Exponential Radial Sampling

All of the following results are new. Instead of choosing $x_{j,k} = \cos^{-1}(k/j)$ or $\cosh^{-1}(k/j)$ as in [5], we choose

$$x_{j,k} = x_{j-k} = \begin{cases} \cos^{-1}\left(e^{\Delta(k-j)}\right), & 1 \le k \le j \\ \cosh^{-1}\left(e^{\Delta(k-j)}\right), & j \le k \le K, \end{cases} \quad (9)$$

and we recall from (6) that $x_{j,0} = \pi/2$ for all j, yielding

$$a_{n,j}(k) = a_n(k) = \frac{p_n(r_{k+1}) - p_n(r_k)}{r_{k+1} - r_k}, \quad (10)$$

which again is clearly a discrete representation of $p_n'(r)$. Defining

$$s_n(j) = \begin{cases} \cos n x_{j-1} - \cos n x_j & j > 0 \\ e^{-n x_{j-1}} - e^{-n x_j} & j \le 0 \end{cases} \quad (11)$$

and substituting in (7), we obtain our main result:

$$\begin{aligned} \mu_n(\rho_j) &= \frac{1}{n\pi} a_n(0)(\cos n x_{j-1} - \cos n\pi/2) \\ &+ \frac{1}{n\pi} \sum_{k=1}^{K-1} a_n(k) s_n(j-k), n, j \neq 0. \quad (12) \end{aligned}$$

Equation (12) computes the exponentially-sampled image harmonics $\mu_n(\rho_j)$ from the exponentially-sampled projection harmonics $p_n(r_k)$. First, (10) "differentiates" $p_n(r_k)$; then the result is convolved with $s_n(j)$ to compute $\mu_n(\rho_j)$ (the first term in (12) is an end effect).

This is analogous to, but different from (33) in [5] in that we are using exponential radial sampling which i) turns the reconstruction problem into convolution, and ii) allows circular harmonic reconstruction method to be used for region-of-interest tomography. Note that (12) cannot be obtained by a simple discretization of the continuous result due to the end effect and sampling points.

For $n = 0$ and $j = 0$, it can be shown that [5]

$$\mu_0(\rho_j) = -\frac{1}{\pi} \sum_{k=j}^{K-1} a_0(k)(x_{j-k-1} - x_{j-k}) \quad (13)$$

and

$$\mu_n(\rho_0) = \mu_n(0) = \begin{cases} -\frac{1}{\pi}\left[2a_0(0) + \Delta \sum_{k=1}^{K-1} a_0(k)\right], & n = 0 \\ 0, & n \neq 0. \end{cases} \quad (14)$$

3.4. Equiangular Sampling

Since we are given $p(r_k, \theta_n)$ for $\theta_n = \frac{2\pi}{N}n, n = 0, \ldots, N-1$, we consider $p(r, \theta) = 0$ for $\theta \neq \frac{2\pi}{N}n$. Since $p(r_k, \theta)$ is discrete and periodic in θ, its Fourier transform is also discrete and periodic. Since by assumption $p(r_k, \theta)$ is angularly bandlimited, (3) becomes the discrete Fourier transform

$$p_n(r_k) = \frac{1}{N} \sum_{l=0}^{N-1} p(r_k, \theta_l) e^{-j\frac{2\pi}{N}nl}, \quad n = -N/2+1, \ldots, N/2. \quad (15)$$

Similarly, (2) also becomes a discrete Fourier transform. To reduce ringing effects caused by the sudden truncation of the circular harmonic expansion (2), we use not (2) but a windowed version of (2)

$$\mu(\rho_j, \phi_l) = \sum_{n=-N/2+1}^{N/2} w_n \mu_n(\rho_j) e^{j\frac{2\pi}{N}nl}, \quad l = 0, \ldots, N-1, \quad (16)$$

where w_n implements a Hamming window.

Finally, we compute the number of operations required to carry out our algorithm. All of the equations can be implemented using the FFT; for $N = K$, this requires $O(N^2 \log N)$ operations. Since both (10) and (12) can be parallelized in n, an even greater computational speedup is possible. By comparison, FBP requires $O(N^3)$ operations to compute the image on a $N \times N$ grid. The computational savings is thus a factor of $O(N/\log N)$.

4. NUMERICAL EXAMPLES

4.1. Numerical Procedures

To demonstrate the effectiveness of our algorithm in achieving high resolution in a region of interest of the image while minimizing artifacts, we present some simulations using the Shepp-Logan phantom. The ROI is defined to consist of the three small ovals at the bottom. Accordingly, the image has been translated in the y-direction by 0.605, so that the small circle, surrounded by two small ovals, is now in the center of the image. All of the images shown in this section are displayed on a 256 × 256 grid, and for the projections $N = 512$ and $K = 128$ (i.e., 128 views at 512 angles). For exponential sampling, $r_1 = 0.01$, $r_K = R = 1.6$, so $\Delta = \ln(1.6/0.01)/127 = 0.040$. To display our reconstructed images, we use a bilinear polar-to-rectangular interpolation algorithm.

Suppose that we are using this interpolation algorithm to display a 256 × 256 image covering the entire phantom. Then pixels far away from the origin of the image will be interpolated using reconstructed polar values $\mu(\rho_j, \phi_n)$ that are not very close to those pixels, while pixels close to the origin of the image will be interpolated using $\mu(\rho_j, \phi_n)$ that are very close to them. In such a situation, many values of $\mu(\rho_j, \phi_n)$ with very small ρ_j will not be used at all in the interpolation to a rectangular grid, since they will not be closest to any pixel. Hence, we may "zoom in" to the origin of the image, i.e., display 256 × 256 images that cover smaller and smaller areas around the origin.

To evaluate our results, we compare them to analogous results obtained using the same number (NK) of samples, but with uniform sampling in r, reconstructed using FBP. The projections $p(r_k, \theta_n)$ are collected for $r_k = \frac{Rk}{K} \times \frac{1}{A}$, $k = 0, \ldots, K-1$; for $r \geq r_K$, we set $p(r, \theta_n) = p(r_{K-1}, \theta_n)$ (this proved to be surprisingly effective, much more effective than setting these values to zero). The parameter A determines the maximum radius that is sampled; as A increases, a smaller region is sampled more finely.

4.2. Discussion of Results

Figs. 1-3 compare results using our algorithm (Figs. 1 and 2) to those using FBP (Fig. 3). The close-up views in Figs. 2 and 3 were obtained as follows. For FBP, we used $A = 8$ to generate Fig. 3. For our algorithm, the excess of $\mu(\rho_k, \theta_n)$ near the origin allows us to "zoom in" to the origin.

In Fig. 1, using our algorithm, note the poor resolution at the top of the image. This is as expected – this region is far from the origin, so its resolution should be poor. But the ROI at the bottom of the image is very sharp.

Zooming in on the ROI in Figs. 2 and 3, our algorithm continues to produce a sharp image, with only a few faint circular artifacts. In contrast, FBP produces an image in which the three ovals are almost washed out. This is the familiar "dishing" artifact, in which the image is artificially bright near its center. Note that this is a very serious error, since the three-oval ROI lies inside another oval, which must also be reconstructed correctly (i.e., the constant but nonzero background must also be reconstructed). It is caused by the infinite support of the FBP filter $h(r)$.

More details on all of these results, including effects of noise, can be found in the full paper [6].

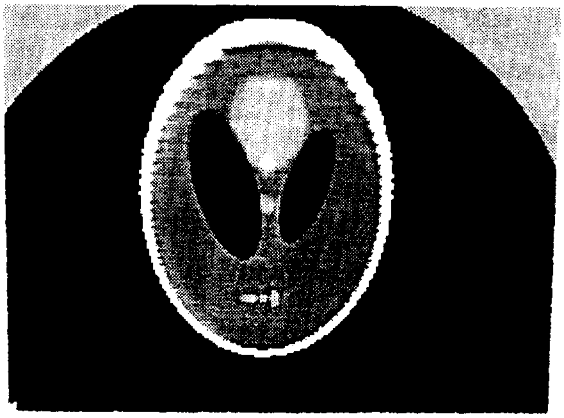

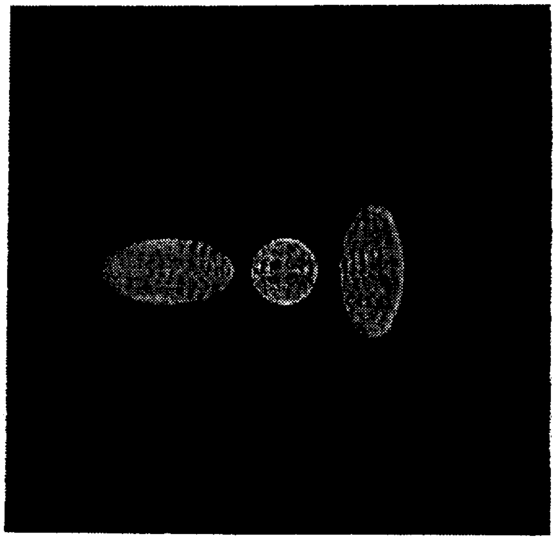

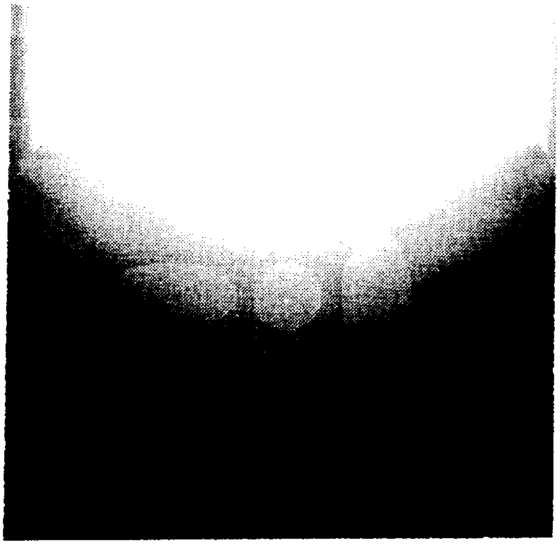

5. REFERENCES

[1] P. Maass, "The interior Radon transform," SIAM J. Appl. Math., vol. 52, pp. 710-724, 1992.

[2] A. Faridani, E. L. Ritman, K. T. Smith, "Local tomography," SIAM J. Appl. Math., vol. 52, pp. 459-484 and 1193-1198, 1992.

[3] J. DeStefano and T. Olson, "Wavelet localization of the Radon transform," IEEE Trans. Sig. Proc., vol. 42, pp. 2055-2067.

[4] A.E. Yagle, "Region of interest tomography using the wavelet transform and angular harmonics," IEEE Sig. Proc. Lett., vol. 1, pp. 134-135.

[5] C. H. Chapman and P. W. Cary, "The circular harmonic Radon transform," Inverse Problems, vol. 2, pp. 23-49, 1986.

[6] B. Sahiner and A.E. Yagle, "Region-of-interest tomography using exponential radial sampling," to appear in IEEE Trans. Image Proc., August 1995.